NASA TECHNICAL MEMORANDUM

NASA TM X-2937

COMPARISON OF PREDICTED AND MEASURED LOW-SPEED PERFORMANCE OF TWO 51-CENTIMETER-DIAMETER INLETS AT INCIDENCE ANGLE

by James A. Albers

Lewis Research Center
Cleveland, Ohio 44135

NATIONAL AERONAUTICS AND SPACE ADMINISTRATION • WASHINGTON, D. C. • NOVEMBER 1973

1. Report No. NASA TM X-2937	2. Government Accession No.	3. Recipient's Catalog No.
4. Title and Subtitle COMPARISON OF PREDICTED AND MEASURED LOW-SPEED PERFORMANCE OF TWO 51-CENTIMETER-DIAMETER INLETS AT INCIDENCE ANGLE		5. Report Date November 1973
		6. Performing Organization Code
7. Author(s) James A. Albers		8. Performing Organization Report No. E-7546
		10. Work Unit No. 501-24
9. Performing Organization Name and Address Lewis Research Center National Aeronautics and Space Administration Cleveland, Ohio 44135		
		11. Contract or Grant No.
		13. Type of Report and Period Covered Technical Memorandum
12. Sponsoring Agency Name and Address National Aeronautics and Space Administration Washington, D.C. 20546		
		14. Sponsoring Agency Code

15. Supplementary Notes

16. Abstract

Theoretical and experimental internal flow characteristics of two 51-cm-diameter inlets are compared. Theoretical flow characteristics along the inlet surface were obtained from an axisymmetric potential flow and boundary layer analysis. The experimental data were obtained from low-speed tests of a high-bypass-ratio turbofan engine simulator. Comparisons between calculated internal surface pressure distributions and experimental data are presented for a free-stream velocity of 45 m/sec and for incidence angles from 0° to 50°. Analysis of boundary layer separation on the inlet lip at incidence angle is the major emphasis of this report. Theoretical boundary layer shape factors, skin friction coefficients, and velocity profiles in the boundary layer are presented, along with the location of the transition region. Theoretical and experimental separation locations are also discussed. Theoretical and experimental static pressures agreed quite well when the inlet flow was attached. Some of the discrepancy between theory and data near the inlet highlight can be explained by the hypothesis of a separation bubble at the inlet lip. Within the limits of the available experimental data and the criteria for establishing experimental separation, reasonable agreement was obtained between the experimental and theoretical location for lip separation.

17. Key Words (Suggested by Author(s)) Engine inlets Boundary layer flow Nacelles Boundary layer transition Potential flow Boundary layer separation Inlet flow	18. Distribution Statement Unclassified - unlimited

19. Security Classif. (of this report) Unclassified	20. Security Classif. (of this page) Unclassified	21. No. of Pages 40	22. Price* Domestic, $3.00 Foreign, $5.50

COMPARISON OF PREDICTED AND MEASURED LOW-SPEED PERFORMANCE
OF TWO 51-CENTIMETER-DIAMETER INLETS AT INCIDENCE ANGLE

by James A. Albers

Lewis Research Center

SUMMARY

This report presents a comparison of theoretical and experimental internal flow characteristics of two 51-centimeter-diameter inlets. Theoretical flow characteristics along the inlet surface were obtained from an axisymmetric potential flow and boundary layer analysis. The experimental data were obtained from low-speed tests of a high-bypass-ratio turbofan engine simulator. Comparisons between calculated internal surface pressure distributions and experimental data are presented for a free-stream velocity of 45 m/sec and for a range of incidence angles from 0° to 50°. Analysis of boundary layer separation on the inlet lip at incidence angle is the major emphasis of this report. Theoretical boundary layer shape factors, skin friction coefficients, and velocity profiles in the boundary layer are presented, along with the location of the transition region. Theoretical and experimental separation locations are also discussed.

Theoretical and experimental static pressures agreed quite well when the inlet flow was attached. Some of the discrepancy between theory and data near the inlet highlight can be explained by the hypothesis of a separation bubble at the inlet lip. Within the limits of the available experimental data and the criteria for establishing experimental separation, reasonable agreement was obtained between the experimental and theoretical location for lip separation.

INTRODUCTION

Accurate methods for estimating surface pressure distributions and boundary layer characteristics are needed for detailed design studies of nacelles and inlets for turbofan engines. These methods should be verified by making comparisons with existing experimental data. A comparison between theoretical internal surface static pressure distributions and experimental data for a 13.97-centimeter-diameter inlet is discussed in reference 1. Good agreement between data and theory was found for conditions where the flow was generally well behaved (i.e., attached along the inlet surface). However,

the boundary layer analysis of reference 1 considered an assumed transition location and turbulent boundary layer growth. These calculations did not predict the separation location on the inlet lip. This report utilizes the potential flow analysis of reference 1. However, it improves the boundary layer analysis by calculating the laminar boundary layer growth and the growth in the transition region from laminar to turbulent flow, as well as the turbulent boundary layer growth.

This report presents a comparison of theoretical and experimental internal flow characteristics of two 51-centimeter-diameter inlets. One inlet had a 1.26-contraction-ratio (highlight area/throat area) inlet lip and the other inlet had a 1.35-contraction-ratio lip. The experimental data were obtained from low-speed tests of a high-bypass-ratio turbofan engine simulator with the two inlets. Comparisons between internal surface pressure distributions and experimental data are presented for a free-stream velocity of 45 m/sec and for a range of incidence angles from 0° to 50°. Comparisons are made for corrected weight flow per unit fan annular areas of 163 and 197 kg/(sec)(m^2), which occur at fan rotational speeds of 90 and 120 percent of design. For the two inlets, these conditions correspond to one-dimensional throat Mach numbers ranging from 0.48 to 0.70.

Analysis of boundary layer separation on the inlet lip is the major emphasis of this report. Theoretical boundary layer shape factors, skin friction coefficients, and velocity profiles in the boundary layer are presented, along with the location of the transition region. Theoretical and experimental separation locations are compared.

APPARATUS

Turbofan Engine Simulator

A high-bypass-ratio turbofan engine simulator was tested with two inlets in the Lewis Research Center's 9- by 15-Foot V/STOL Propulsion Wind Tunnel. The model is shown in figure 1. The model has a 50.8-centimeter-diameter single-stage fan driven by a four-stage axial-flow turbine supplied with high-pressure air. The fan has a 1.15 pressure ratio and a 0.4 hub- to tip-diameter ratio.

Inlet Designs

The two inlet configurations considered in this report are shown in figures 2 and 3. Both inlets have the same highlight diameter and maximum diameter of 51.06 and 54.62 centimeters, respectively. The external forebody geometries were NACA-1 series

2

contours (ref. 2), and the internal lip contours were 2-to-1 ellipses. Reference 3 indicates that an internal ellipse with a major- to minor-axis ratio of 2.0 was nearly optimum for the contraction ratios considered in this report. The inlet diffusers were designed so the maximum surface angle did not exceed 10°. The diffuser exit Mach number was 0.6 at a fan rotational speed of 100 percent of design, corresponding to a corrected weight flow per unit fan annular area of 176 kg/(sec)(m^2).

The difference in the internal lip geometries is in the lip contraction ratio (i. e., highlight area/throat area). One inlet has a 1.35 contraction ratio (fig. 2) and the other has a 1.26 contraction ratio (fig. 3). The 1.35-contraction-ratio inlet has an overall length of 36 centimeters, while the 1.26-contraction-ratio inlet has a length of 28.16 centimeters. The cowl and spinner coordinates are given in figures 2 and 3.

METHOD OF ANALYSIS

Computer Programs

The inlet potential and viscous flows were obtained by use of four computer programs (fig. 4). The first program, SCIRCL (ref. 4), establishes the coordinates and point spacing on the inlet surfaces. The second program, EOD, is the Douglas axisymmetric incompressible potential flow program. The method is discussed in detail in reference 5. The program EOD is used to obtain three basic solutions for flow around inlets. These solutions are used as the input to a third computer program, called COMBYN. The method of this program is described in detail in reference 6. It combines the basic solutions to obtain a solution for any combination of free-stream velocity, inlet incidence angle, and mass flow rate through the inlet. The program COMBYN also corrects the incompressible potential flow solution for compressibility by the method described in reference 7. The surface Mach number distributions obtained from the program COMBYN are used as an input to the fourth program, VISCUS, which calculates the boundary layer growth and separation point (if any) on the inlet surface. The program VISCUS is a modified version of the Herring and Mellor program (ref. 8), which calculates the laminar and turbulent boundary layer development in compressible flow. However, in reference 8, the location of the transition point was a program input. (In ref. 1, the transition point was assumed to take place at the point of minimum pressure on the surface of the inlet.) In this report, the transition region was determined by the empirical correlations of reference 9.

Transition. - Theoretical investigations into the process of transition from laminar to turbulent flow are based on Reynolds' hypothesis that transition occurs as a consequence of an instability developed within the laminar boundary layer. The transition region is defined as the region between the instability point (or critical point) and the fully turbulent point. The instability point is the point on the surface at which amplification of some individual disturbances begin and proceed downstream. The boundary layer becomes fully turbulent some distance downstream of the instability point since the disturbance takes time to amplify to fully developed turbulent flow.

The physical factors which influence the transition location that have been accounted for in this analysis include pressure gradient, surface roughness, free-stream turbulence level, and longitudinal curvature. The point of instability is determined from the critical Reynolds number R_{cr}, which is a function of the pressure gradient parameter $\overline{K}$.

$$R_{cr} = f(\overline{K}) \tag{1}$$

where

$$\overline{K} = \frac{\theta^2}{\nu_w} \frac{dU}{ds}$$

(All symbols are defined in the appendix.)

The difference between the Reynolds number at the fully turbulent point R_{ft} and the critical Reynolds number R_{cr} is a function of both the pressure gradient parameter and the free-stream turbulence level $\overline{q^2}/U^2$, where

$$R_{ft} - R_{cr} = R_\Delta(\overline{K}) f\left(\frac{\overline{q^2}}{U^2}\right) \tag{2}$$

If the effect of longitudinal curvature θ/r and surface roughness S_w/δ^* are included, the Reynolds number at the fully turbulent point becomes

$$R_{ft} = \left[R_{cr}(\overline{K}) + R_\Delta(\overline{K}) f\left(\frac{\overline{q^2}}{U^2}\right)\right] f\left(\frac{\theta}{r}\right) f\left(\frac{S_w}{\delta^*}\right) \tag{3}$$

All the functional relationships of equations (1) and (3) were obtained from reference 9. For this investigation the inlet surface was taken as smooth ($S_w/\delta^* = 0$), and the turbulence intensity was assumed to be 0.9 percent. The wind tunnel turbulence level was obtained from reference 10.

The effective viscosity in the transition region is determined from the kinematic viscosity ν, the intermittency factor γ, and the turbulent viscosity ν_t.

$$\nu_e = \nu + \gamma \nu_t \tag{4}$$

The intermittency factor is defined as that fraction of time during which the flow at a given position remains turbulent. It was calculated from the method of reference 11.

Separation. - It is important that the development of the laminar and turbulent boundary layer be accurately determined to ascertain whether the boundary layer would separate and, if so, at what point on the inlet surface. The point of separation is defined as the point where the wall shear stress is equal to zero, that is,

$$\tau_w = \mu_e \left(\frac{\partial u}{\partial y} \right)_w = 0 \tag{5}$$

Zero wall shear stress gives zero skin friction coefficient, which is defined as

$$C_f = \frac{\tau_w}{\frac{1}{2}\rho U^2}$$

Another condition of the point of separation is a large increase in shape factor as the separation point is approached. The shape factor H is defined as the ratio of displacement thickness to momentum thickness. It is desirable to minimize the value of the shape factor and unfavorable (increasing) local shape factor gradients. The flatter the distribution of the shape factor along the inlet surface, the less likelihood of obtaining boundary layer separation. In the integral methods of Cohen and Reshotko (ref. 12) and Evans (ref. 13), laminar separation theoretically takes place when the shape factor H reaches a value of 4.03. In integral methods, turbulent separation of the flow theoretically occurs when H reaches a value between 1.8 and 2.4 (ref. 14). However, for finite difference methods, such as the one used in this investigation, the separation point could correspond to different values of H than the values indicated by the integral methods. The values of H near separation are established herein as typical examples of separated flow are discussed.

DISCUSSION OF RESULTS

Experimental surface static pressure distributions are compared with potential flow pressure distributions first for the 1.35-contraction-ratio inlet, for which the flow is attached for the greater range of test conditions, and then for the 1.26-contraction-

ratio inlet. The effects of both circumferential angle and incidence angle on internal surface pressure distributions are illustrated, followed by a discussion of the boundary layer characteristics for attached and separated flow cases.

Potential Flow Pressure Distributions

Effect of circumferential angle. - The effect of circumferential angle on the surface static pressure distribution is presented in figure 5 for a free-stream velocity of 45 m/sec and an incidence angle of 30°. The throat corrected specific weight flow, w_{cor}/A_F = 163 kg/(sec)(m^2), occurs at a fan rotational speed of 90 percent of design. These conditions correspond to one-dimensional throat Mach numbers of 0.48 for the 1.26-contraction-ratio inlet and 0.51 for the 1.35-contraction-ratio inlet. The pressure distributions are presented from the inlet highlight (X/L = 0) to the diffuser exit (X/L = 1.0). The circumferential variation in static pressure is greatest at the inlet highlight (X/L = 0) and decreases with increasing X/L. The lowest static pressures occur at a circumferential angle of 0°. Larger surface Mach numbers, at a circumferential angle of 0°, were obtained for the 1.26-contraction-ratio inlet (fig. 5(b)) than for the 1.35-contraction-ratio inlet (fig. 5(a)). The experimental static pressures generally compare well with the theoretical pressures for all circumferential angles. This agreement indicates attached flow along the inlet surface for both inlet configurations for incidence angles to 30°. The slight differences between data and theory in the aft portion of the diffuser (X/L > 0.6) can be attributed to the neglect of the boundary layer displacement thickness in the potential flow solution, as is shown in reference 1. Good agreement over the entire length of the diffuser was obtained in reference 1 when the boundary layer displacement thickness was accounted for.

All remaining comparisons will be made at a circumferential angle of 0° since the maximum surface Mach numbers occur and flow separation begins at this location.

Effect of incidence angle. - The effect of incidence angle is illustrated in figure 6 for the 1.35-contraction-ratio inlet at corrected flow rate to fan annular area ratios (w_{cor}/A_F) of 163 and 197 kg/(sec)(m^2) and for incidence angles ranging from 0° to 50°. Surface static pressures are presented from the stagnation point (X/L < 0) to the diffuser exit (X/L = 1.0). (At a free-stream velocity of 45 m/sec the stagnation point occurs on the external surface, which is shown as a negative value of X/L.)

Good agreement between data and theory is obtained at an incidence angle of 0° (fig. 6(a)). However, as incidence angle increases, the experimental static pressures in the region of the inlet lip (0 < X/L < 0.1) are higher than the predicted pressures. At an incidence angle of 10° (fig. 6(b)) the experimental static pressure increases immediately downstream of the inlet highlight and then decreases as the inlet throat location is approached. At an incidence angle of 20° (fig. 6(c)), this same characteristic is

observed, with the deviation between data and theory getting progressively larger at the higher incidence angles. This result is most evident for incidence angles of 30° and 40° (figs. 6(d) and (e)) at a corrected weight flow to fan annular area ratio of 197 kg/(sec)(m^2). For X/L greater than 0.1, relatively good agreement is obtained between data and theory. This result can be attributed to a small region of separation on the inlet lip, followed by reattachment of the boundary layer. The separation bubble gets progressively bigger as incidence angle is increased from 10° to 40° but disappears at an incidence angle of 50° for a corrected flow rate to fan annular area ratio of 197 kg/(sec)(m^2) (fig. 6(f)).

Good agreement between data and theory is obtained even for local Mach numbers to 2.0. However, for an incidence angle of 50° and a corrected flow rate to fan annular area ratio of 163 kg/(sec)(m^2) (fig. 6(f)), the experimental static pressures are much higher than predicted on the inlet lip (0 < X/L < 0.2) and much lower than predicted in the inlet diffuser. This discrepancy between data and theory is interpreted to mean that a separated flow originates on the inlet lip and extends down the length of the diffuser. For a separated flow condition the static pressures are relatively flat from inlet highlight to diffuser exit. By using this as a criterion for experimental lip separation, the location of separation is determined as shown in figure 6(f).

The effect of incidence angle on the 1.26-contraction-ratio inlet is illustrated in figure 7. Similarly, good comparisons with data and theory were obtained for this inlet configuration for incidence angles from 0° to 30° (figs. 6(a) to (d)).

Some evidence of a small separation bubble followed by reattachment near the inlet highlight is illustrated at an incidence angle of 30° (fig. 7(d)). At an incidence angle of 40° and 50° (figs. 7(e) and (f)), the experimental static pressures are relatively flat from inlet highlight to diffuser exit. The theoretical potential flow static pressures predict a large adverse gradient in the inlet throat. Examination of the experimental and theoretical pressure distributions indicates separation very near the inlet highlight for corrected flow rate to fan annular area ratios of 163 and 197 kg/(sec)(m^2).

In summary, figures 6 and 7 indicate that theory and experimental data agree quite well when the inlet flow is attached and if one hypothesizes a separation bubble at the inlet lip to account for some of the disagreements between theory and data near the inlet highlight. Inlet separation as a function of incidence angle is readily identifiable from the changes in static pressure distribution when separation occurs.

The following section uses the theoretically predicted surface Mach numbers and a boundary layer analyses to predict the inlet separation.

Boundary Layer Characteristics

Typical theoretical Mach number distributions and boundary layer parameters are plotted against the fractional distance from the stagnation point to the diffuser exit

s/s_{max} in figure 8 for the 1.26-contraction-ratio inlet. The boundary layer parameters presented are the shape factor H, the skin friction coefficient C_f, and the boundary layer velocity profiles. Also shown, were applicable, is the predicted location of the transition region, along with the theoretical and experimental separation location. Calculated results are presented at a free-stream velocity of 45 m/sec and one-dimensional throat Mach numbers of 0.48 and 0.64. Calculations are made for incidence angles ranging from 0° to 50°.

Inlet contraction ratio, 1.26; throat Mach number, 0.48. - At an incidence angle of 0° (fig. 8(a)) the surface Mach number gradients are relatively mild, with a peak Mach number of 0.7. The transition region occurs downstream of the inlet highlight ($X/L = 0$). The transition region is defined as the distance between the instability point and the fully turbulent point. The instability point occurs very near the peak Mach number location for all conditions investigated. The peak Mach number occurs very near the inlet high-light for incidence angles of 20° and greater. At an incidence angle of 30° (fig. 8(b)) the adverse Mach number gradient is larger, with a peak Mach number of 1.36. This results in the fully turbulent point moving closer to the instability point as incidence angle in-creases. Examination of figures 8(a) to (d) indicates that the higher the Mach number level on the inlet surface, the closer the transition region moves toward the inlet high-light.

For all incidence angles the value of the laminar shape factor H is 2.2 at the stagna-tion point ($s/s_{max} = 0$) and increases as the transition region is approached. At an inci-dence angle of 0° (fig. 8(a)), H increases to 2.85 downstream of the instability point and then decreases to a value of approximately 1.7 at the fully turbulent point. The shape factor remains relatively constant along the diffuser surface. At an incidence angle of 30° (fig. 8(b)), H reaches a value of 3.95 just downstream of the instability point and then decreases to a value of 2.05 at the fully turbulent point. This is followed by a relatively constant value of H along the diffuser, except for an increase near s/s_{max} of 0.85. Ex-amination of figures 8(c) and (d) indicates that, as incidence angle is increased, both the level and gradient of the shape factor increase in both the laminar and turbulent regions of the boundary layer.

The skin friction coefficient decreases sharply in the laminar portion of the flow in the region of the large unfavorable Mach number gradient immediately downstream of the inlet highlight. In the turbulent portion of the flow, there is a more gradual decrease in the skin friction coefficient along the inlet surface (figs. 8(a) to (c)). Zero skin friction coefficient was not obtained for incidence angles of 0° and 30° (figs. 8(a) and (b)), indi-cating attached flow for these conditions.

The velocity profiles in the boundary layer at various locations along the surface are also illustrated in figure 8. The profiles shown downstream of the stagnation point are typical laminar and turbulent profiles. For attached flow (figs. 8(a) and (b)), the predominant change in the velocity profiles along the inlet surface is the change associated

with the change from laminar to turbulent boundary layer. For separated and very nearly separated flows (figs. 8(c) and (d)), there is a much greater change in the velocity profiles, as would be expected.

For incidence angles of 40° and 50° (figs. 8(c) and (d)), the experimental and theoretical separation locations are illustrated. The experimental separation locations were obtained by examination of the static pressure distributions of figures 7(e) and (f). The theoretical separation locations were determined from the location at which the skin friction coefficient was approximately zero (0.00005 or less). The experimental separation locations in figures 8(c) and (d) occur very near the inlet highlight. For an incidence angle of 40° (fig. 8(c)), the theoretical separation location occurs downstream of the inlet highlight at an s/s_{max} of 0.72. However, theoretical separation is almost obtained near the inlet highlight, where a skin friction coefficient of 0.0002 is obtained with a corresponding shape factor of 4.6. Thus, the maximum value of the shape factor that was observed without having lip separation is approximately 4.6. At an incidence angle of 50° (fig. 8(d)), the separation occurs ahead of the fully turbulent point, indicating laminar separation on the inlet lip. The theoretical shape factor at the separation point is 5.25.

Inlet contraction ratio, 1.26; throat Mach number, 0.64. - The boundary layer parameters for the 1.26-contraction-ratio inlet with the one-dimensional throat Mach number of 0.64 are presented in figure 9. These curves result in much higher Mach number levels and gradients than the curves illustrated for the 1.26-contraction-ratio inlet with the one-dimensional throat Mach number of 0.48 in figure 8. At an incidence angle of 20° (fig. 9(a)), the peak Mach number is 1.5, with a relatively large adverse Mach number gradient. Since no separation is obtained, the boundary layer parameters are very similar to the attached flow cases of figure 8. The laminar shape factor on the inlet lip reaches a peak value of 4.03 at the inlet highlight, with a corresponding skin friction coefficient of 0.001.

At an incidence angle of 30° (fig. 9(b)), the peak Mach number is 2.0, followed by a large adverse Mach number gradient. The theoretical analysis predicted laminar lip separation near the inlet highlight (fig. 9(b)). However, no separation was evident experimentally. Examination of static pressure data of figure 7(d) indicates a separation bubble near the inlet highlight, followed by reattachment of the boundary layer. Because of the complexity of predicting reattachment of the boundary layer, the reattachment phenomenon was not considered in this analysis.

At incidence angles of 40° and 50° (figs. 9(c) and (d)), both theoretical and experimental separation locations occur very near the inlet highlight. The velocity profiles represented in figures 9(c) and (d) are representative of laminar separation profiles.

Inlet contraction ratio, 1.35. - Theoretical Mach number distributions and boundary layer parameters for the 1.35-contraction-ratio inlet are presented in figure 10. At an incidence angle of 40°, lip separation was not observed experimentally for one-

dimensional throat Mach numbers of 0.51 and 0.70 (figs. 10(a) and (b)). However, theoretical diffuser separation was predicted at an s/s_{max} of approximately 0.75. Examination of the static pressure distributions of figures 6(d) and (e) indicates generally attached flow along the inlet surfaces. However, the increase in spread between the experimental static pressures and theory in the diffuser from 30° to 40° incidence angle indicates the possibility of diffuser separation near an s/s_{max} of 0.8.

At an incidence angle of 50° with a one-dimensional throat Mach number of 0.51 (fig. 10(c)), theoretical separation was almost obtained near the inlet highlight, where a skin friction coefficient of 0.0006 was predicted. Examination of the pressure distributions of figure 6(f) shows lip separation near the inlet highlight for a one-dimensional throat Mach number of 0.51. Lip separation was also predicted at a one-dimensional throat Mach number of 0.70 (fig. 10(d)). Examination of the pressure distribution of figure 6(f) for a throat Mach number of 0.70 does not clearly indicate lip separation.

Separation summary. - A summary of the comparison of the experimental and theoretical lip separation results for both inlets is illustrated in figures 11 and 12. The figures show the incidence angle range where attached flow and lip separation occur theoretically and experimentally. Since the experimental data were taken in 10-degree increments, the exact incidence angle where lip separation occurs could not be determined. The theoretical calculations were made over a smaller range of incidence angles.

For the 1.26-contraction-ratio inlet (fig. 11), attached flow was obtained experimentally to an incidence angle of 30°. Lip separation was obtained experimentally for incidence angles of 40° and above. These results apply for a one-dimensional throat Mach number of 0.48 (fig. 11(a)) and for a one-dimensional throat Mach number of 0.64 (fig. 11(b)). For a one-dimensional throat Mach number of 0.48 (fig. 11(a)), lip separation was obtained theoretically at an incidence angle of 41° and above. For a one-dimensional throat Mach number of 0.64 (fig. 11(b)), lip separation was obtained theoretically at an incidence angle of 29° and above.

For the 1.35-contraction-ratio inlet, attached flow was obtained experimentally at incidence angles to 40° at a one-dimensional throat Mach number of 0.51 (fig. 12(a)), and to 50° at a one-dimensional throat Mach number of 0.70 (fig. 12(b)). Attached flow was obtained theoretically at incidence angles to 50° at a one-dimensional throat Mach number of 0.51 (fig. 12(a)) and to 44° at a one-dimensional throat Mach number of 0.70 (fig. 12(b)).

Because of the 10-degree increments in which data were taken, the correspondence between the experimental and theoretical separation angle could range between $\pm 1^O$ to $\pm 11^O$.

SUMMARY OF RESULTS

The predicted and measured low-speed performances of two inlets were compared. One inlet had a 1.35-contraction-ratio (highlight area/throat area) inlet lip and the other inlet had a 1.26-contraction-ratio inlet lip. Theoretical flow characteristics along the inlet surface were obtained from an axisymmetric potential flow and boundary layer analysis. Internal surface static pressure distributions were compared at a free-stream velocity of 45 m/sec and a range of incidence angles from 0° to 50°, with an average throat Mach number ranging from 0.48 to 0.70. Theoretical boundary layer shape factors, skin friction coefficients, boundary layer velocity profiles, location of the transition region, and experimental and theoretical separation locations were presented. The principal results of this study are as follows:

1. Theoretical and experimental static pressures agreed quite well when the inlet flow was attached. Some of the discrepancy between theory and data near the inlet highlight can be explained by the hypothesis of a separation bubble at the inlet lip. Good agreement between data and theory was obtained for local Mach numbers on the inlet lip as high as 2.0.

2. Inlet lip separation as a function of incidence angle was readily identifiable from the changes in static pressure distribution when separation occurred. For lip separation, the experimental static pressures were relatively flat from inlet highlight to diffuser exit, while the theoretical pressure distributions predicted large adverse pressure gradients on the lip surface.

3. The inlet flow remained attached for both inlets for incidence angles to 30°. For the 1.35-contraction-ratio inlet, the flow remained attached for all conditions except an incidence angle of 50° with a one-dimensional throat Mach number of 0.51. For the 1.26-contraction-ratio inlet the flow separated near the inlet highlight at incidence angles of 40° and 50° for all throat Mach numbers investigated.

4. The transition region is the distance between the instability point and the fully turbulent point. The calculated instability point occurred very near the maximum Mach number location for all conditions investigated. The calculated fully turbulent point moved closer to the instability point as incidence angle increased. The maximum Mach number occurred very near the inlet highlight for incidence angles of 20° and greater.

5. As incidence angle increased, both the level and gradient in the shape factor increased in both the laminar and turbulent regions of the boundary layer. The value of the laminar shape factor before lip separation occurred ranged from 4.0 to 4.6. The flatter the distribution of the shape factor δ^*/θ along the inlet surface, the less likelihood of obtaining boundary layer separation.

6. Within the limits of the available experimental data and the criteria for establishing experimental separation, reasonable agreement was obtained between the experimental and theoretical locations for lip separation.

Lewis Research Center,
National Aeronautics and Space Administration,
Cleveland, Ohio, August 7, 1973,
501-24.

APPENDIX - SYMBOLS

A   area

A_1/A_T inlet contraction ratio

C_f skin friction coefficient

D   diameter

H   shape factor, δ^*/θ

$\overline{K}$ pressure gradient parameter

L   distance from inlet highlight to diffuser exit (fig. 2)

M   Mach number

$\widetilde{M}$ one-dimensional Mach number at throat plane

N   fan rotational speed

R   Reynolds number

r   longitudinal curvature

P   total pressure

p   static pressure

$\overline{q^2}/U^2$ turbulence intensity

S_w characteristics of roughness elements

s   local surface distance from stagnation point

U   velocity at outer edge of boundary layer (potential flow velocity)

u   velocity in boundary layer

X   distance from inlet highlight (fig. 2)

Y   distance from inlet axis (fig. 2)

y   coordinate normal to surface

w   weight flow rate

α incidence angle

γ intermittency factor

δ boundary layer thickness

δ^* displacement thickness

θ momentum thickness

μ	molecular viscosity
ν	kinematic viscosity
ρ	density
τ	local shear stress
ψ	circumferential angle around inlet

Subscripts:

cor	corrected
cr	critical point
e	effective
F	fan annulus
ft	fully turbulent point
max	maximum
T	throat
t	turbulent
w	wall
Δ	fully turbulent point minus critical point
∞	free stream
1	highlight

REFERENCES

1. Albers, James A.: Theoretical and Experimental Internal Flow Characteristics of a 13.97-Centimeter-Diameter Inlet at STOL Takeoff and Approach Conditions. NASA TN D-7185, 1973.

2. Baals, Donald D.; Smith, Norman, F.; and Wright, John B.: The Development and Application of High-Critical-Speed Nose Inlets. NACA Rep. 920, 1948.

3. Albers, James A.; and Miller, Brent A.: Effect of Subsonic Inlet Lip Geometry on Predicted Surface and Flow Mach Number Distributions. NASA TN D-7446, 1973.

4. Stockman, Norbert O.; and Button, Susan L.: Computer Programs for Calculating Potential Flow in Propulsion Systems Inlets. NASA TM X-68278, 1973.

5. Hess, J. L.; and Smith, A. M. O.: Calculation of Potential Flow About Arbitrary Bodies. Progress in Aeronautical Sciences, Vol. 8, D. Küchemann, ed., Pergamon Press, 1967, pp. 1-138.

6. Stockman, Norbert O.: Potential Flow Solutions for Inlets of VTOL Lift Fans and Engines. Analytic Methods in Aircraft Aerodynamics. NASA SP-228, 1970, pp. 659-681.

7. Lieblein, S.; and Stockman, N. O.: Compressibility Correction for Internal Flow Solutions. J. Aircraft, vol. 9, no. 4, Apr. 1972, pp. 312-313.

8. Herring, H. J.; and Mellor, G. L.: Computer Program for Calculating Laminar and Turbulent Boundary Layer Development in Compressible Flow. NASA CR-2068, 1972.

9. Schlichting, Hermann (J. Kestin, trans.): Boundary-Layer Theory. Sixth ed., McGraw-Hill Book Co., Inc., 1968.

10. Yuska, Joseph A.; Diedrich, James H.; and Clough, Nestor: Lewis 9-by-15-Foot V/STOL Wind Tunnel. NASA TM X-2305, 1971.

11. Dhawan, S.; and Narasimha, R.: Some Properties of Boundary Layer Flow During the Transition From Laminar to Turbulent Motion. J. Fluid Mech., vol. 3, pt. 4, Jan. 1958, pp. 418-436.

12. Cohen, Clarence B.; and Reshotko, Eli: The Compressible Laminar Boundary Layer with Heat Transfer and Arbitrary Pressure Gradient. NACA Rep. 1294, 1956.

13. Evans, Harry L.: Laminar Boundary-Layer Theory. Addison-Wesley Publ. Co., 1968, p. 70.

15. Cebeci, T.; Mosinski, G. J.; and Smith, A. M. O.: Calculation of Separation Points in Incompressible Turbulent Flows. J. Aircraft, vol. 9, no. 5, Sept. 1972, pp. 618-624.
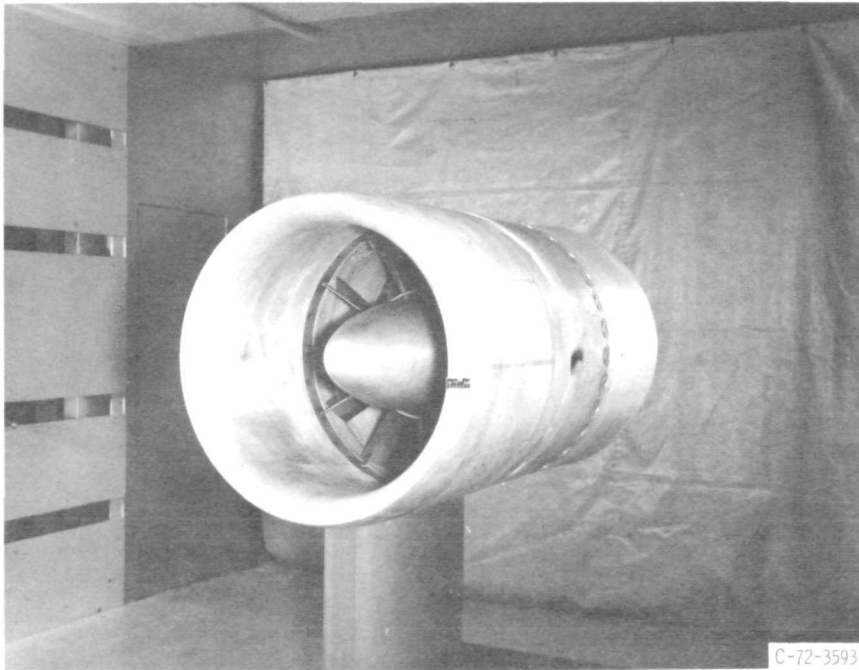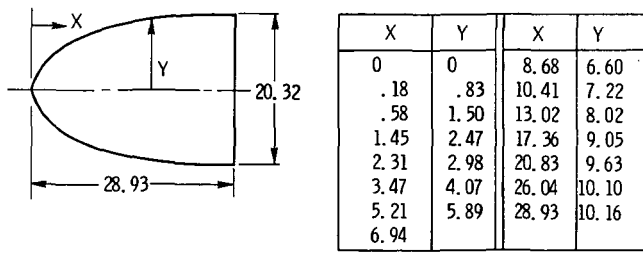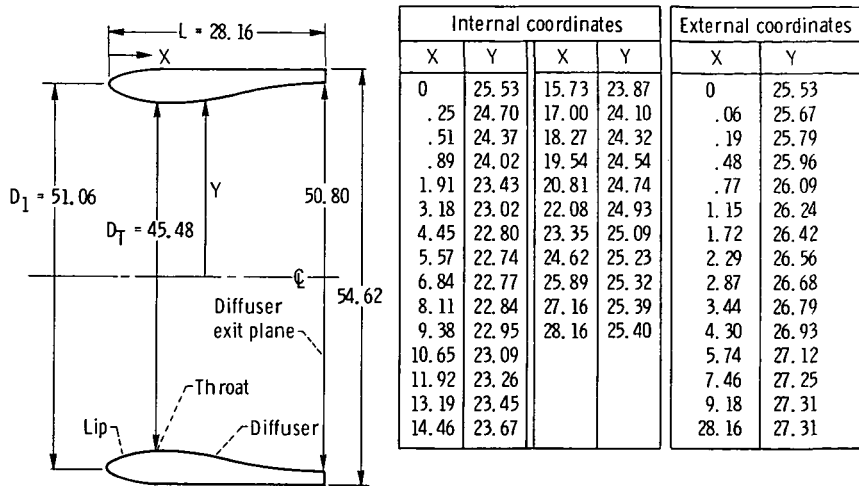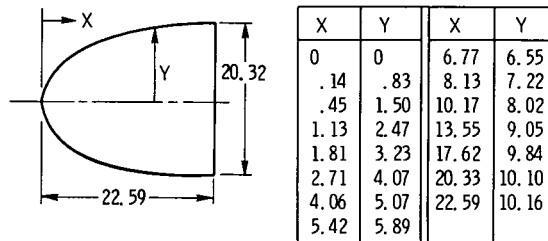
Figure 1. - Turbofan engine simulator.

Internal coordinates		External coordinates	
X	Y	X	Y
0	25.53	0	25.53
.46	24.27	.06	25.67
.93	23.79	.19	25.79
1.62	23.78	.48	25.96
3.00	22.64	.77	26.09
4.62	22.21	1.15	26.24
7.07	22.00	1.72	26.42
9.38	22.06	2.29	26.56
11.68	22.23	2.87	26.68
13.99	22.49	3.44	26.79
16.30	22.82	4.30	26.93
18.61	23.19	5.74	27.12
20.92	23.59	7.46	27.25
23.23	24.00	9.18	27.31
25.54	24.39	36.00	27.31
27.53	24.75		
29.00	24.90		
31.31	25.16		
33.62	25.34		
36.00	25.40		

(a) Cowl.

X	Y	X	Y
0	0	8.68	6.60
.18	.83	10.41	7.22
.58	1.50	13.02	8.02
1.45	2.47	17.36	9.05
2.31	2.98	20.83	9.63
3.47	4.07	26.04	10.10
5.21	5.89	28.93	10.16
6.94			

(b) Spinner.

Figure 2. – Details of cowl and spinner design for inlet contraction ratio A_1/A_T of 1.35. (Dimensions are in centimeters.)

(a) Cowl.

Internal coordinates				External coordinates	
X	Y	X	Y	X	Y
0	25.53	15.73	23.87	0	25.53
.25	24.70	17.00	24.10	.06	25.67
.51	24.37	18.27	24.32	.19	25.79
.89	24.02	19.54	24.54	.48	25.96
1.91	23.43	20.81	24.74	.77	26.09
3.18	23.02	22.08	24.93	1.15	26.24
4.45	22.80	23.35	25.09	1.72	26.42
5.57	22.74	24.62	25.23	2.29	26.56
6.84	22.77	25.89	25.32	2.87	26.68
8.11	22.84	27.16	25.39	3.44	26.79
9.38	22.95	28.16	25.40	4.30	26.93
10.65	23.09			5.74	27.12
11.92	23.26			7.46	27.25
13.19	23.45			9.18	27.31
14.46	23.67			28.16	27.31

X	Y	X	Y
0	0	6.77	6.55
.14	.83	8.13	7.22
.45	1.50	10.17	8.02
1.13	2.47	13.55	9.05
1.81	3.23	17.62	9.84
2.71	4.07	20.33	10.10
4.06	5.07	22.59	10.16
5.42	5.89		

(b) Spinner

Figure 3. – Details of cowl and spinner design for inlet contraction ratio A_1/A_T of 1.26. (Dimensions are in centimeters.)
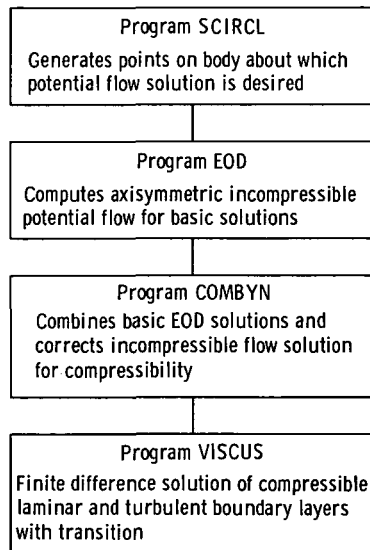
Figure 4. – Schematic representation of computer programs.

$\psi = 180^0$

30^0 ℄

U_∞

$\psi = 0^0$

Circumferential angle, ψ, deg

○	0 ⎫
△	90 ⎬ Experiment
□	180 ⎭
——	0 ⎫
– – –	90 ⎬ Theory
–·–·–	180 ⎭
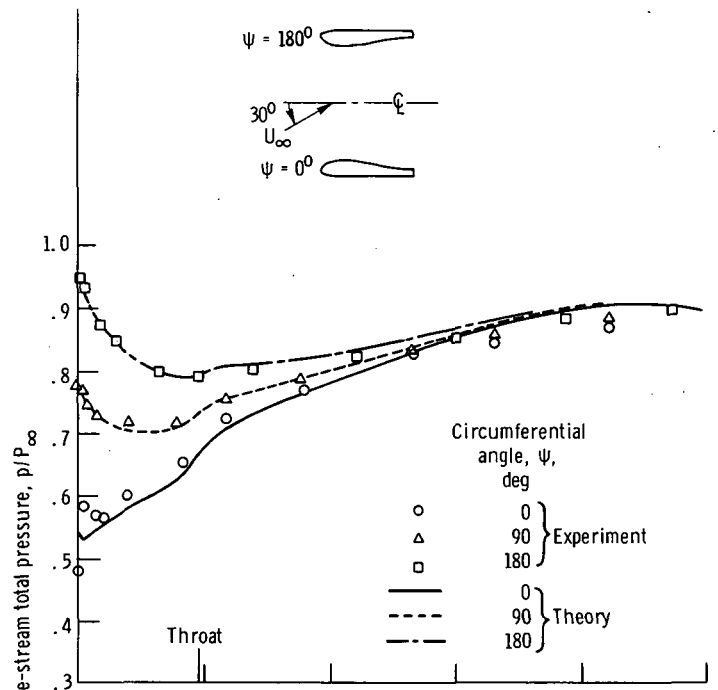
Throat

(a) Inlet contraction ratio, A_1/A_T, 1.35; one-dimensional throat Mach number, $\overline{M}$, 0.51.

Throat

Fractional distance from highlight, X/L
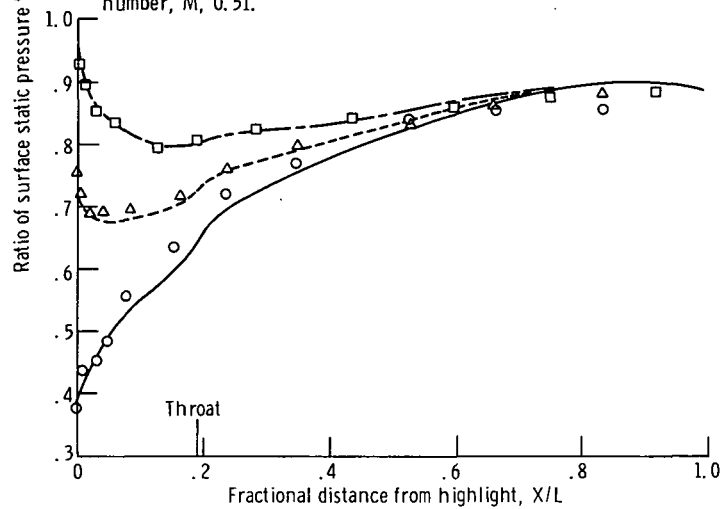
(b) Inlet contraction ratio, A_1/A_T, 1.26; one-dimensional throat Mach number, $\overline{M}$, 0.48.

Figure 5. - Potential flow surface static pressure distributions for various circumferential angles. Free-stream velocity, 45 m/sec; incidence angle, 30^0; ratio of corrected flow rate to annular area, 163 kg/(sec)(m^2); fan speed, 90 percent of design.

Ratio of surface static pressure to free-stream total pressure, p/P_∞

		Ratio of corrected flow rate to fan annular area, w_{cor}/A_F, kg/(sec)(m²)	Fan speed, N, percent of design	One-dimensional throat Mach number, $\bar{M}$
Experiment	○	163	90	0.51
	□	197	120	.70
Theory	——	163	90	.51
	—·—	197	120	.70

(a) Incidence angle, 0⁰.

(b) Incidence angle, 10⁰.

(c) Incidence angle, 20⁰.
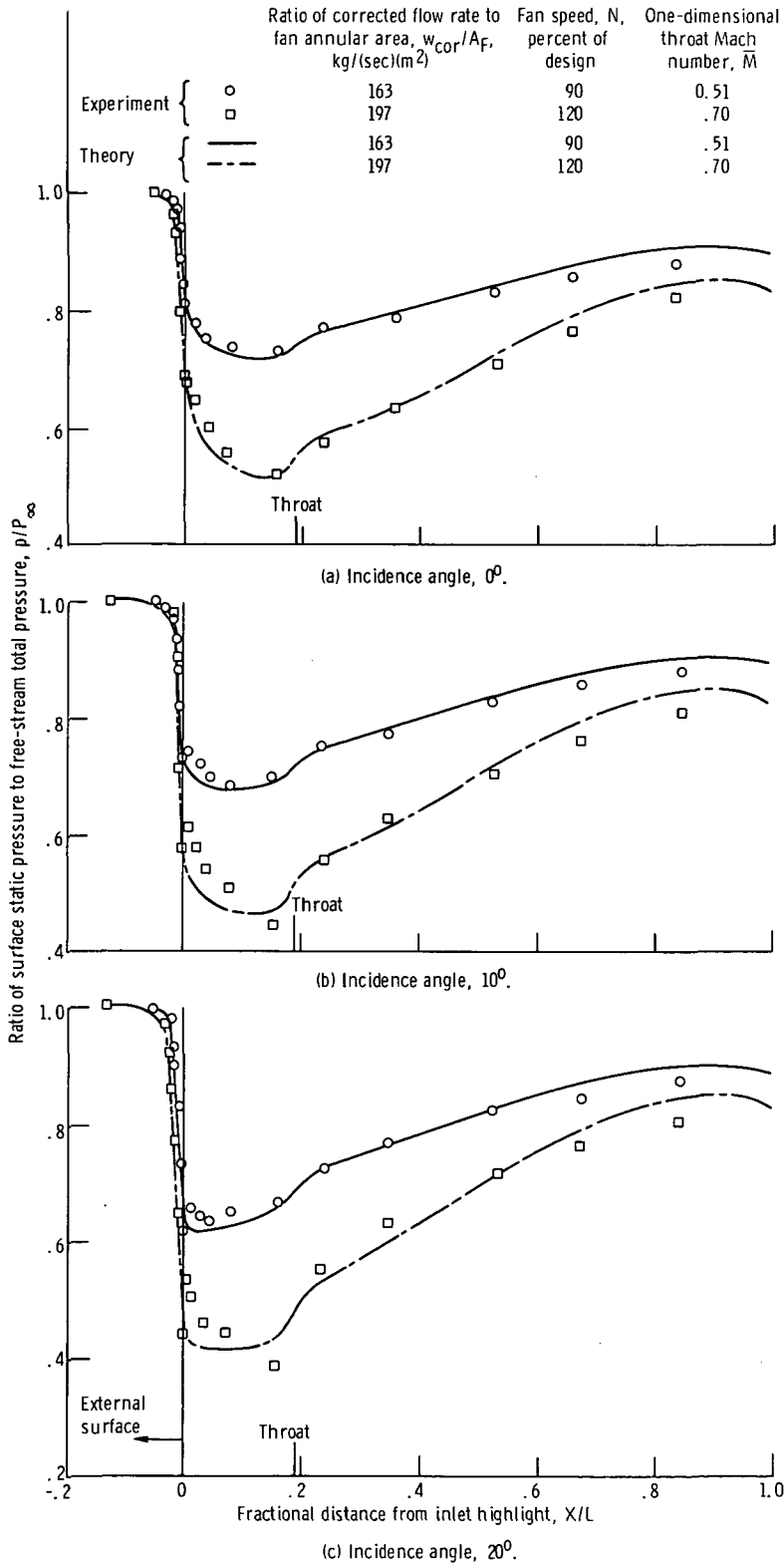
Figure 6. – Effect of incidence angle on potential flow surface static pressure distribution for 1.35-contraction-ratio inlet. Free-stream velocity, 45 m/sec; circumferential angle, ψ, 0⁰.

Figure 6.- Continued.

(d) Incidence angle, 30⁰ appears on the figure as "(d) incidence angle, 30⁰."

		Ratio of corrected flow rate to fan annular area, w_{cor}/A_F, kg/(sec)(m²)	Fan speed, N, percent of design	One-dimensional throat Mach number, M
Experiment {	○	163	90	0.51
	□	197	120	.70
Theory {	——	163	90	.51
	—·—·—	197	120	.70

(f) Incidence angle, 50°.

Figure 6. - Concluded.
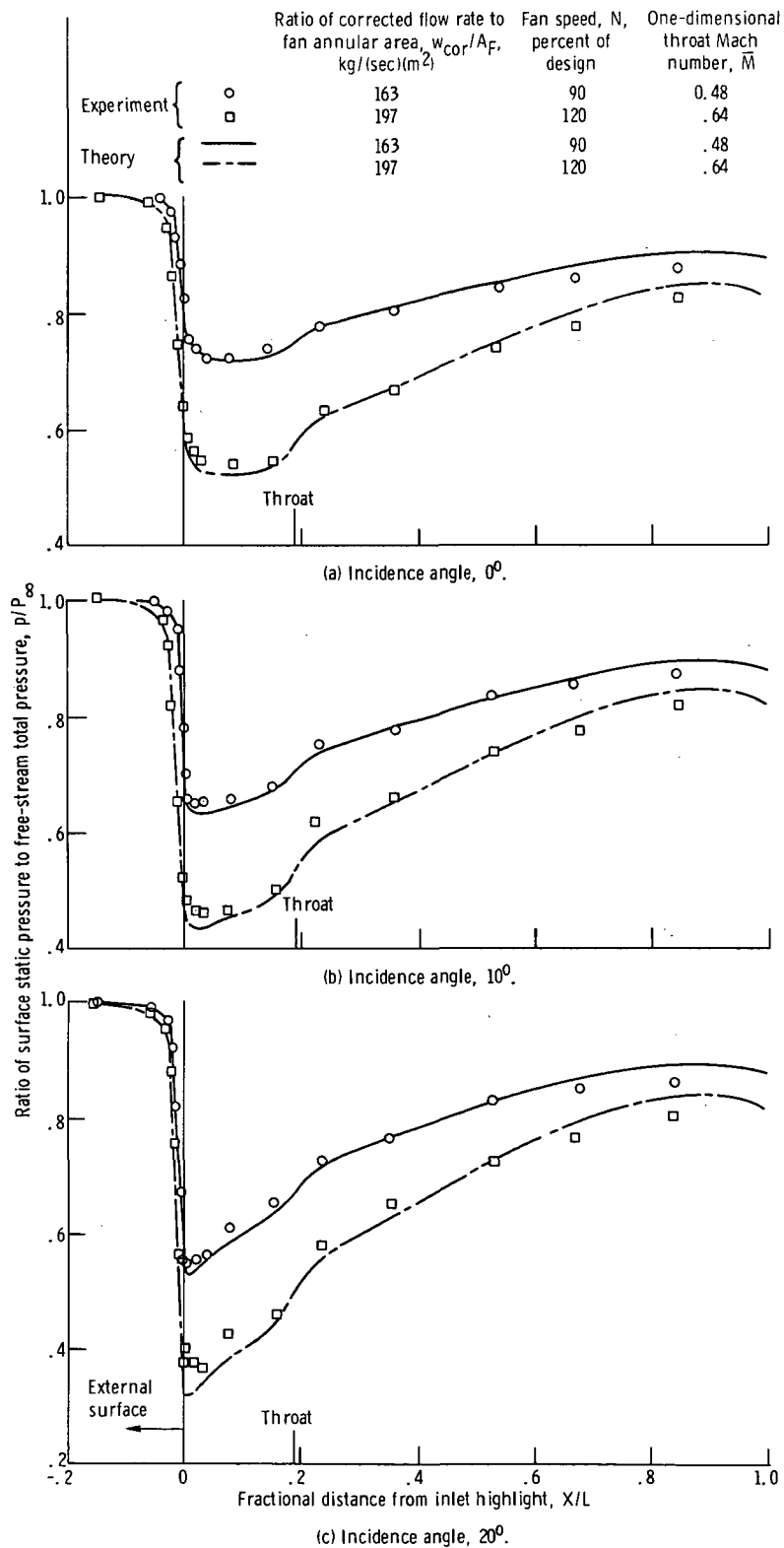
Figure 7. - Effect of incidence angle on potential flow surface static pressure distribution for 1.26-contraction-ratio inlet. Free-stream velocity, 45 m/sec; circumferential angle, ψ, 0°.

Ratio of corrected flow rate to | Fan speed, N, | One-dimensional
fan annular area, w_{cor}/A_F, | percent of | throat Mach
kg/(sec)(m^2) | design | number, $\bar{M}$

Experiment
- ○   163   90   0.48
- □   197   120   .64

Theory
- ———   163   90   .48
- – – –   197   120   .64

Ratio of surface static pressure to free-stream total pressure, p/P_∞

Throat

(d) Incidence angle, 30°.

Experimental separation location ($\bar{M} = 0.48$)

Experimental separation location ($\bar{M} = 0.64$)

External surface

Throat

-.2   0   .2   .4   .6   .8   1.0

Fractional distance from inlet highlight, X/L

(e) Incidence angle, 40°.

Figure 7. – Continued.

(f) Incidence angle, 50°.

Figure 7. - Concluded.

(a) Incidence angle, 0^0; no experimental separation.
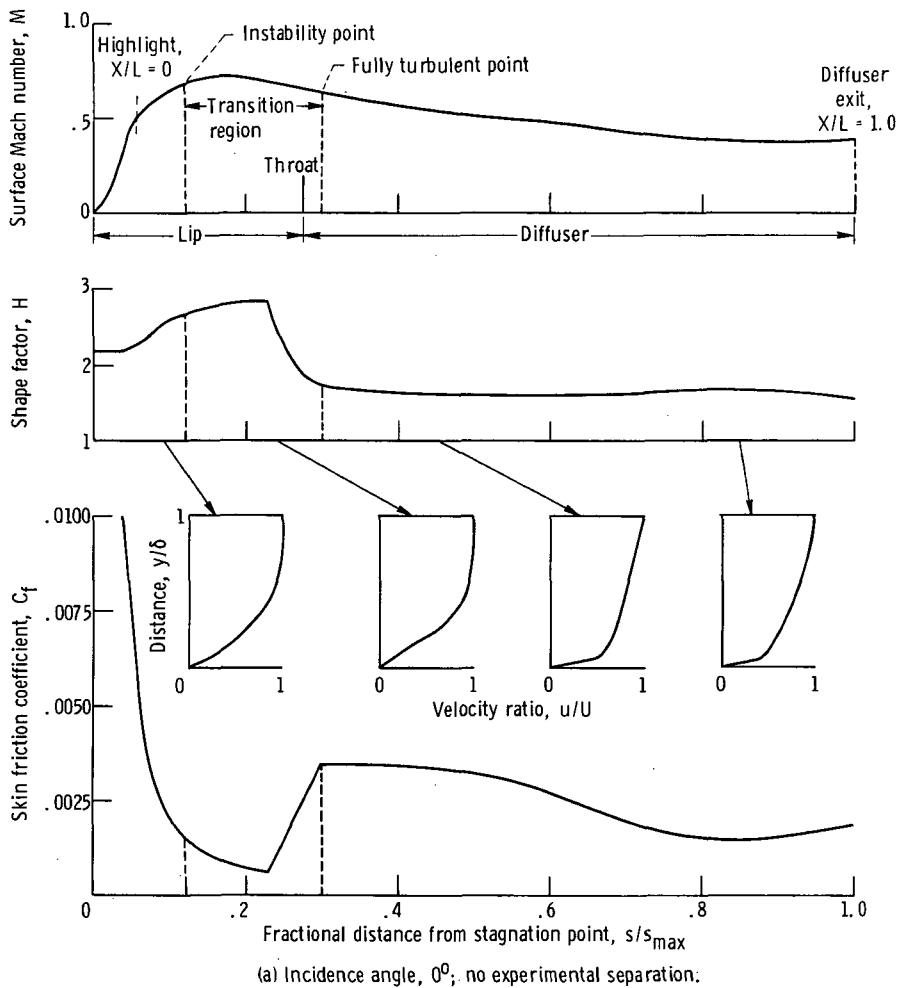
Figure 8. – Theoretical Mach number distributions and boundary layer parameters for 1.26-contraction-ratio inlet, free-stream velocity of 45 m/sec, circumferential angle of 0^0, and one-dimensional Mach number of 0.48.

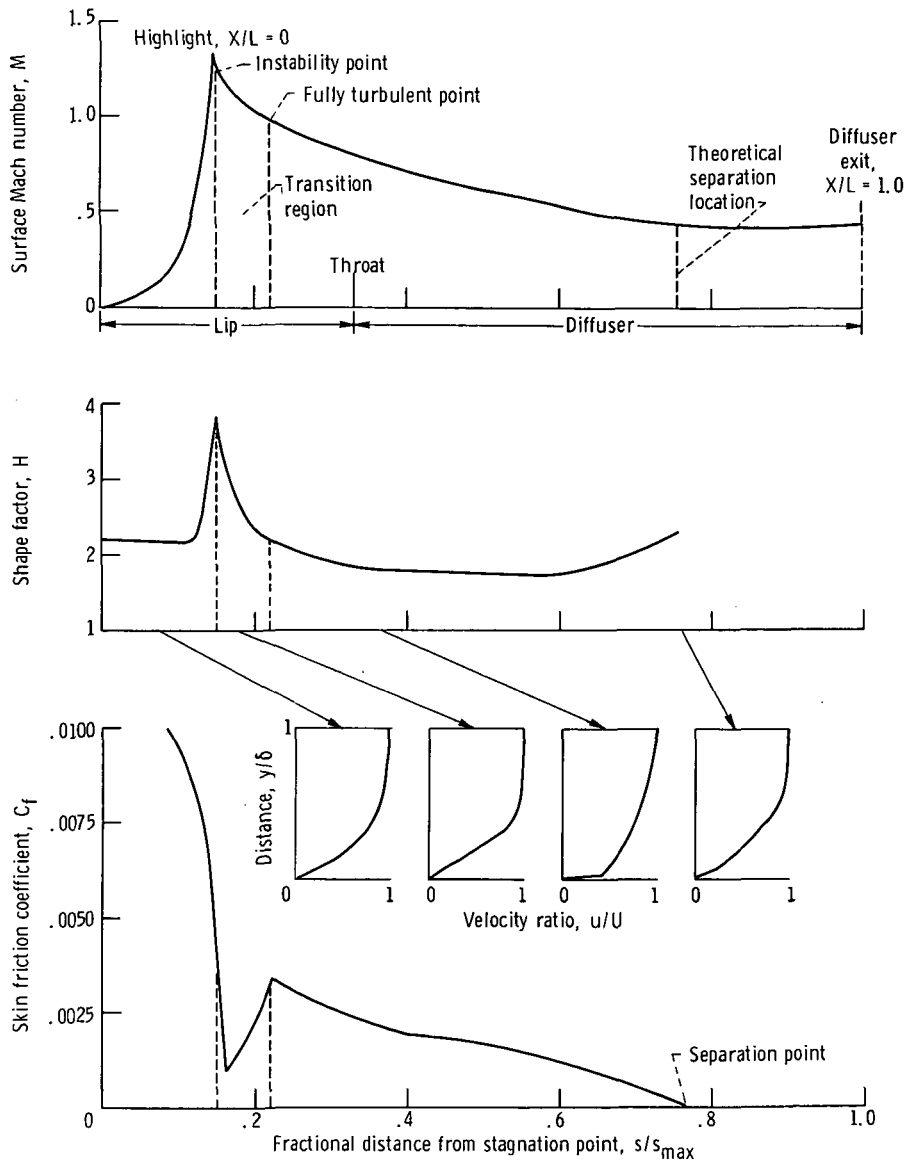(b) Incidence angle, 30°; no experimental separation.

Figure 8. - Continued.

28
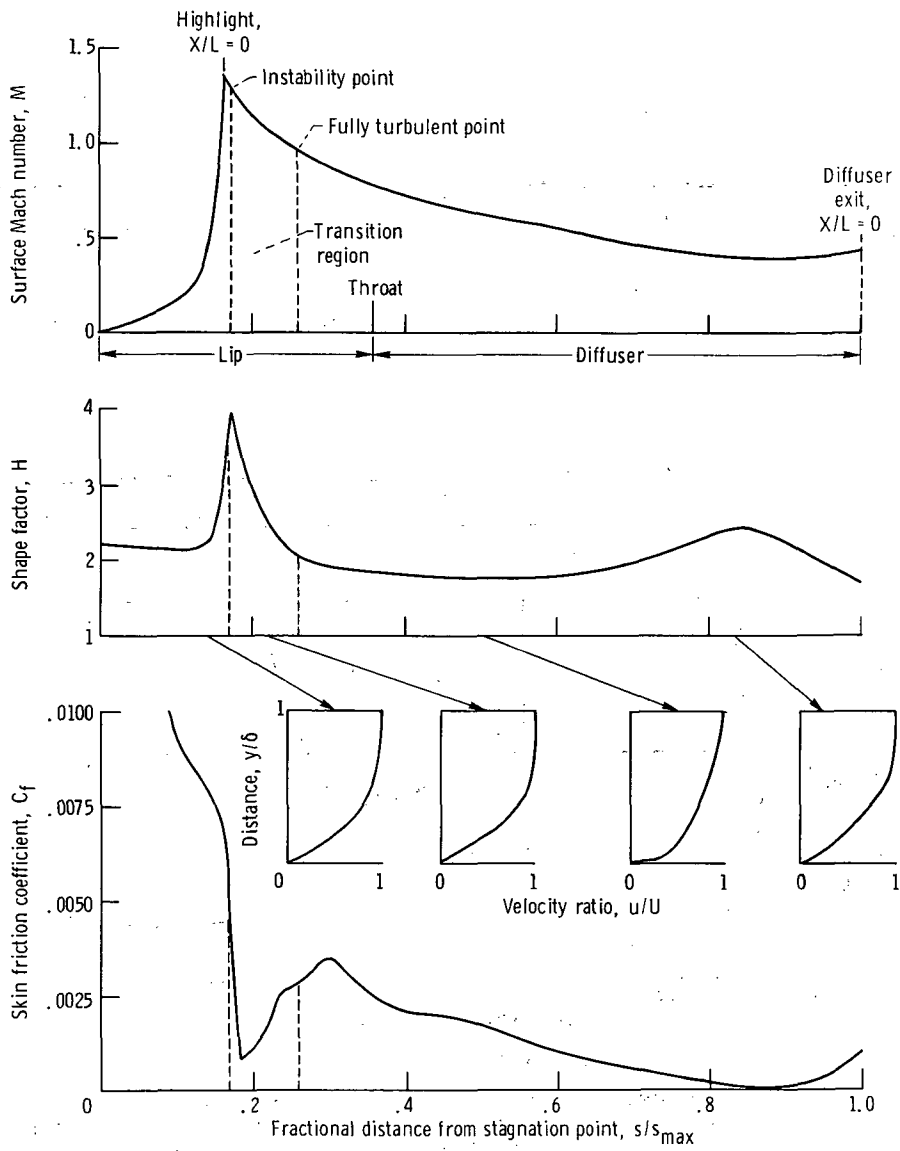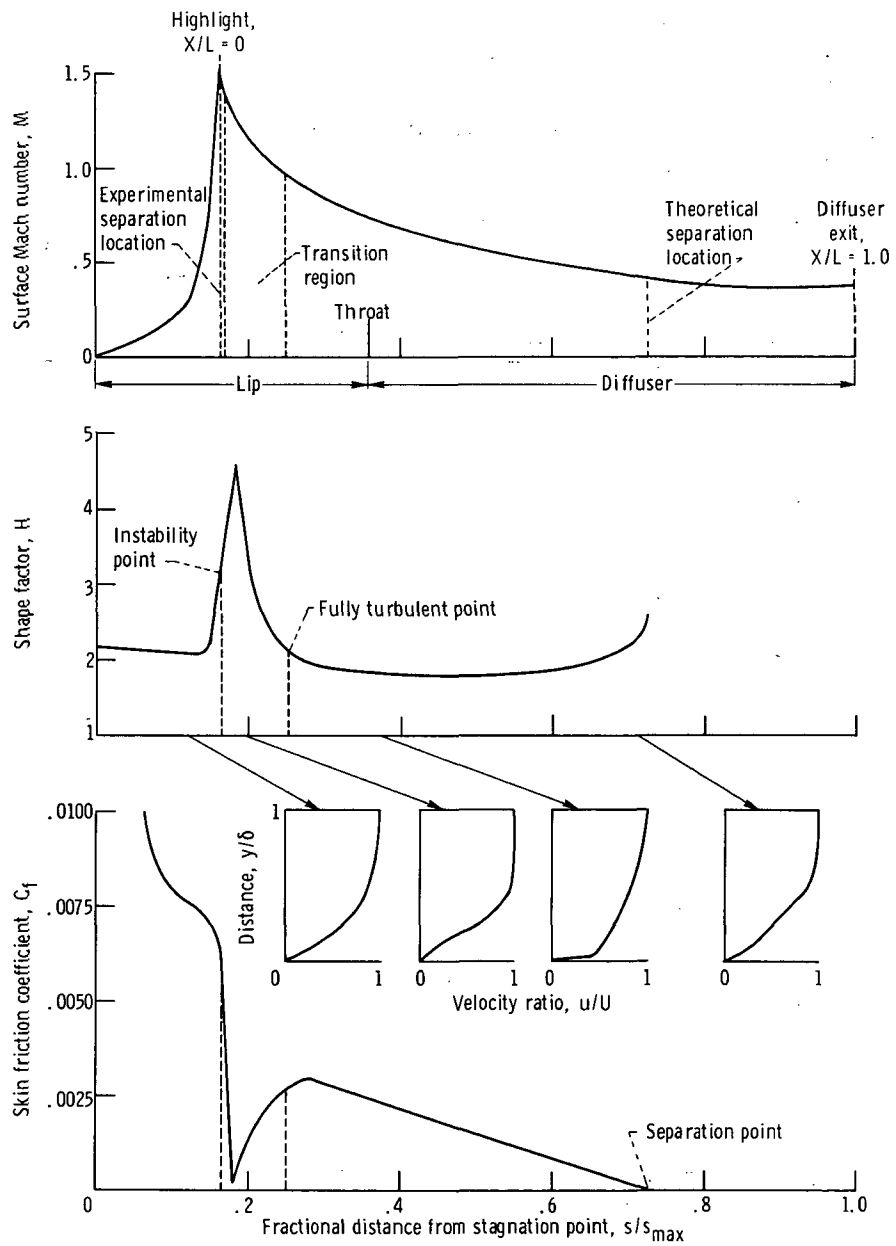
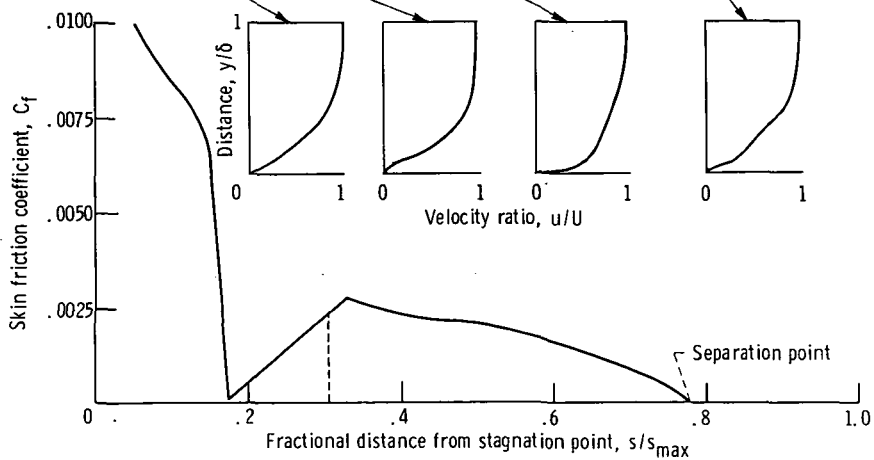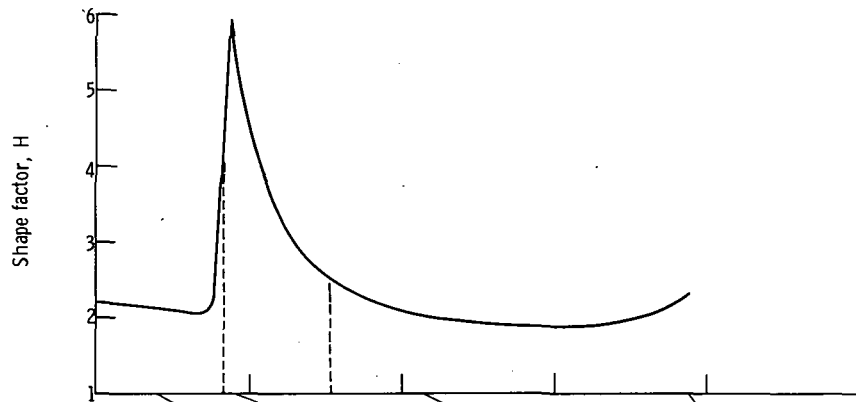(c) Incidence angle, 40°; experimental separation.

Figure 8. - Continued.

(d) Incidence angle, 50^0; experimental separation.

Figure 8. - Concluded.
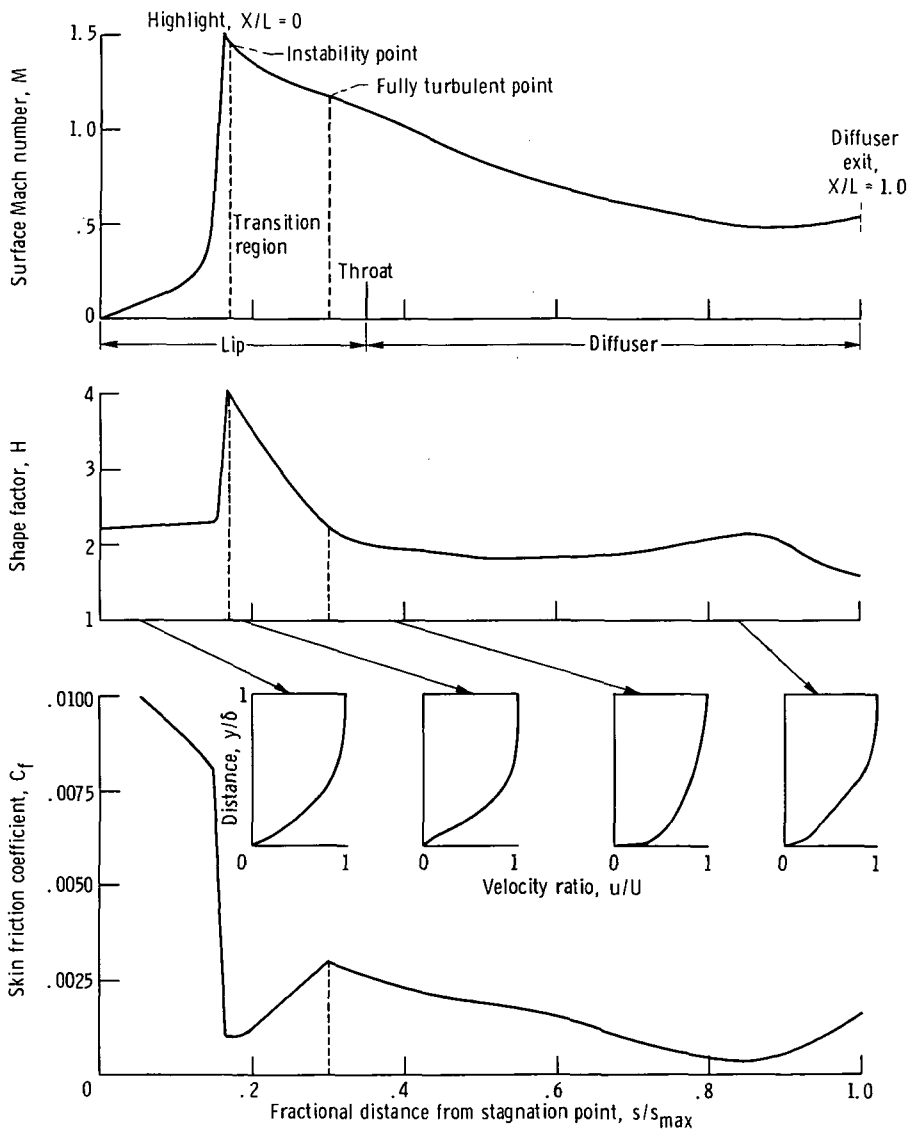
(a) Incidence angle, 20°; no experimental separation.

Figure 9. - Theoretical Mach number distributions and boundary layer parameters for 1. 26-contraction-ratio inlet, free-stream velocity of 45 m/sec, circumferential angle of 0°, and one-dimensional Mach number of 0. 64.
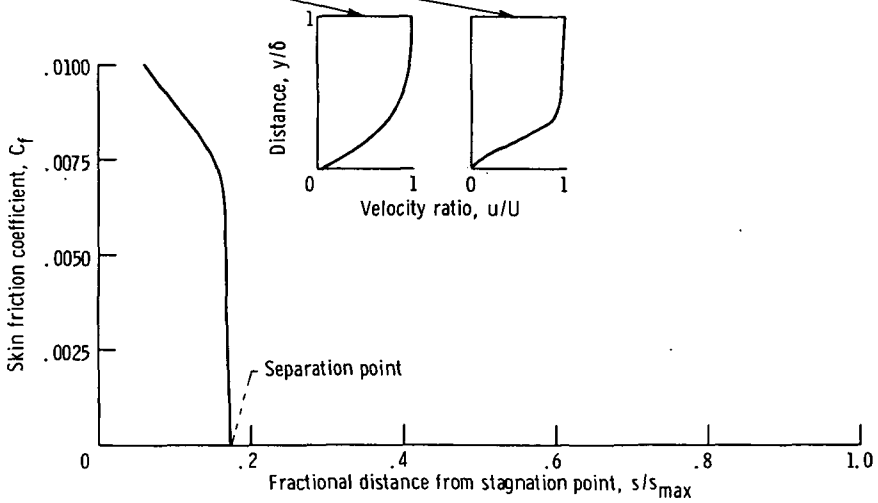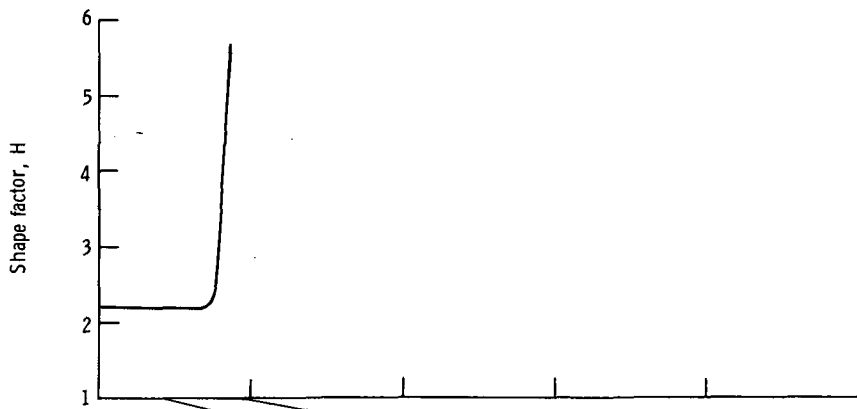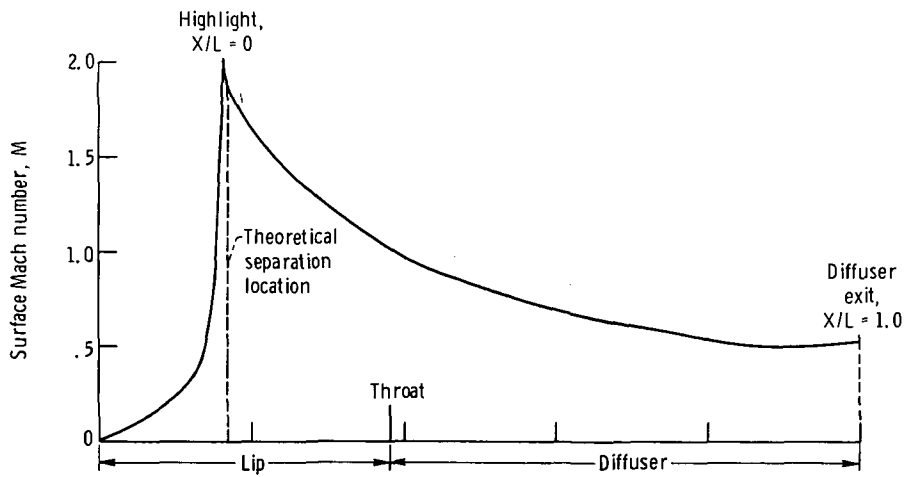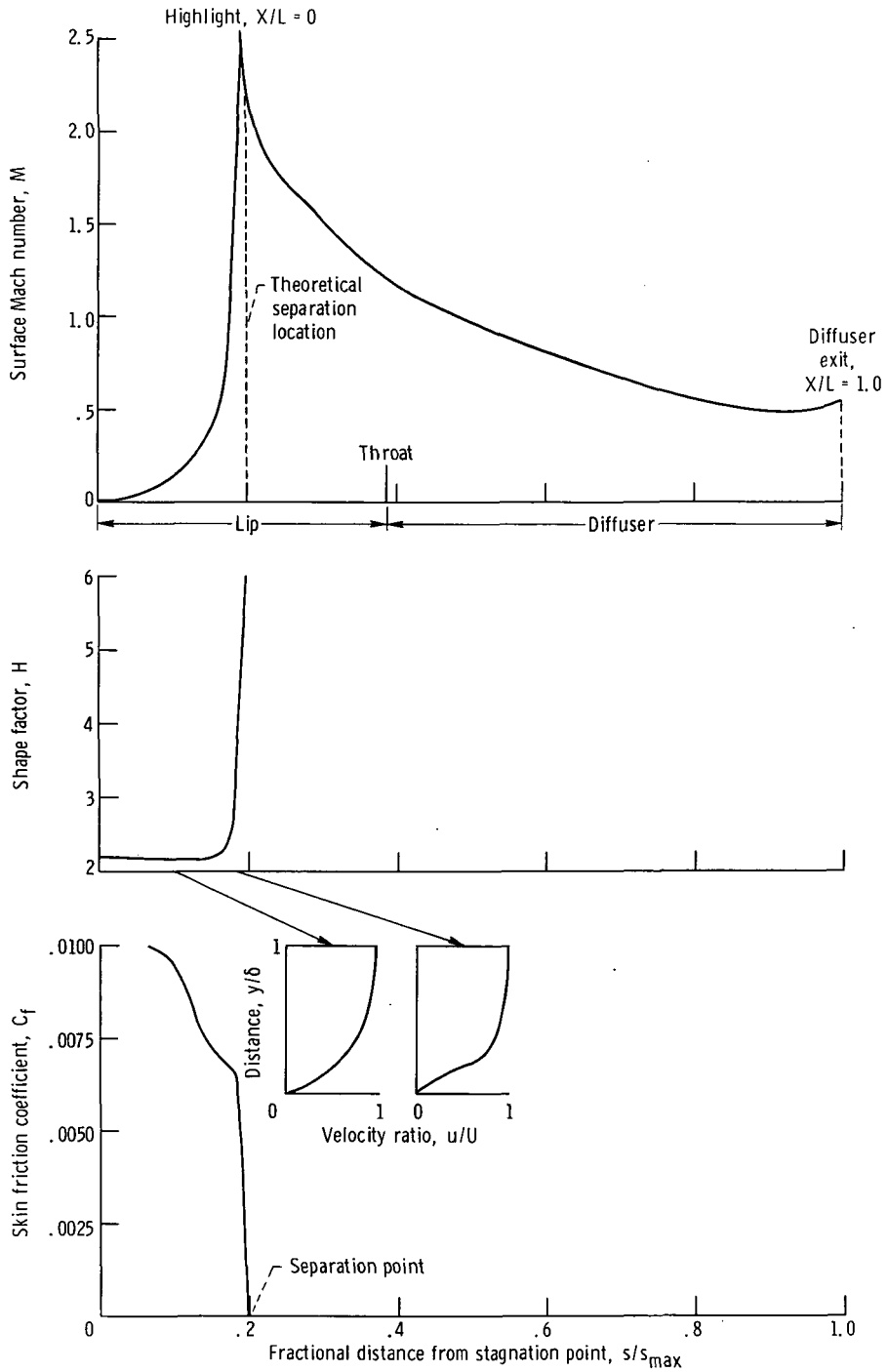
(b) Incidence angle, 30°; no experimental separation.

Figure 9. – Continued.

(c) Incidence angle, 40^0; experimental separation.

Figure 9. - Continued.

(d) Incidence angle, 50°; experimental separation.

Figure 9. - Concluded.

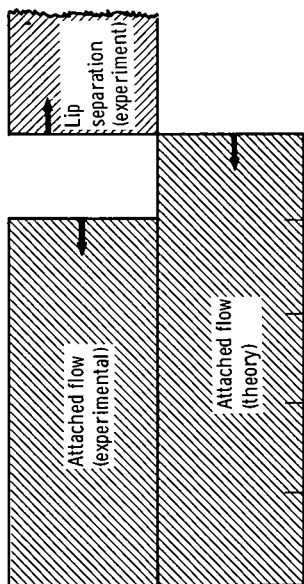(a) Incidence angle, 40°; one-dimensional throat Mach number, 0.51; no experimental separation.

Figure 10. - Theoretical Mach number distributions and boundary layer parameters for 1.35-contraction-ratio inlet, free-stream velocity of 45 m/sec, and circumferential angle of 0°
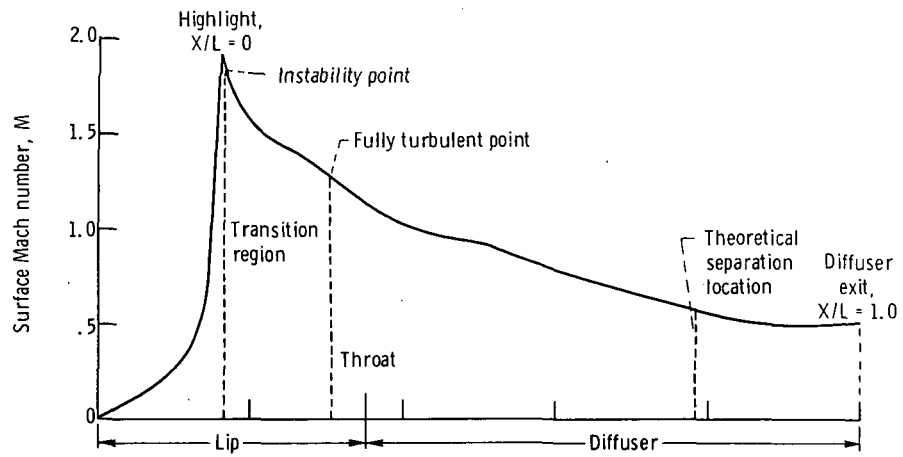
(b) Incidence angle, 40°; one-dimensional throat Mach number, 0.70; no experimental separation.

Figure 10. – Continued.
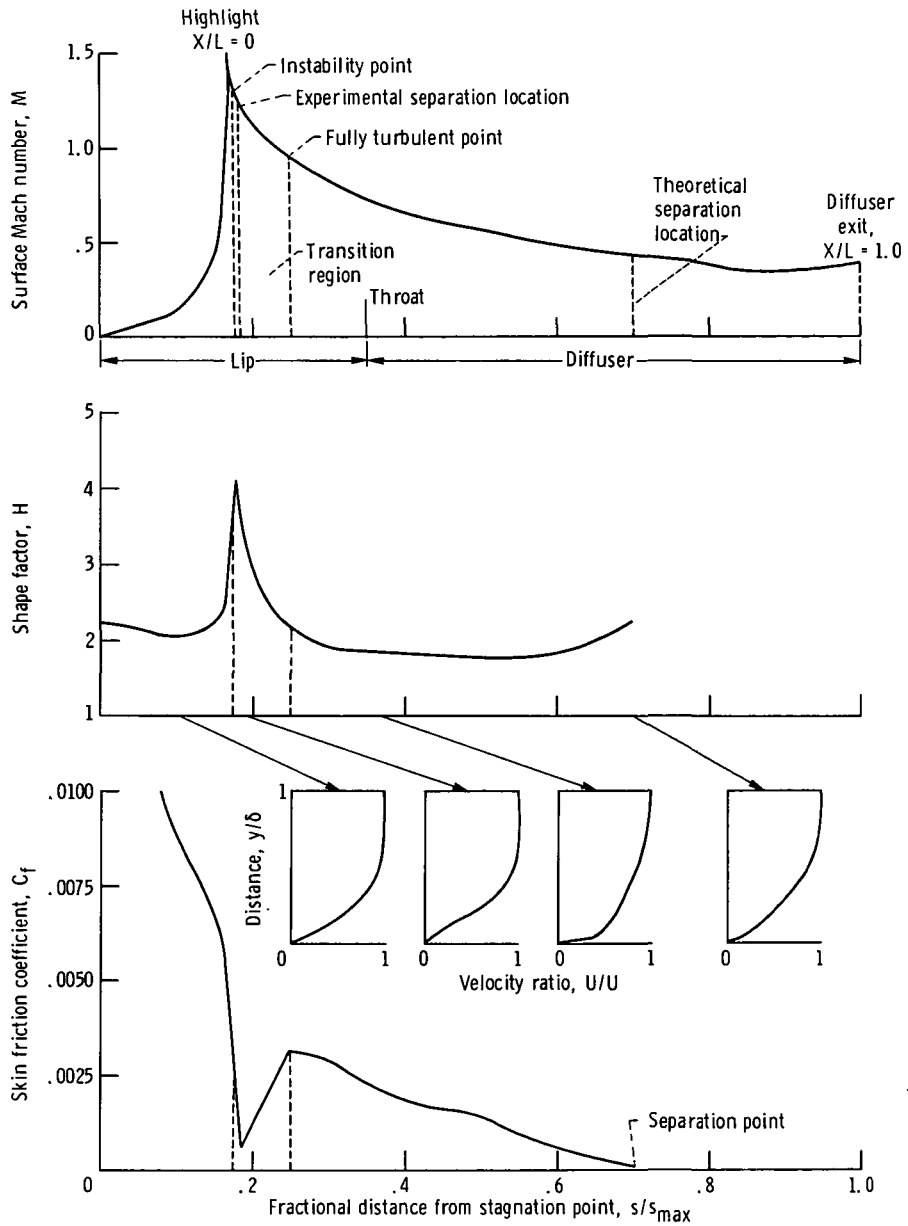
(c) Incidence angle, 50°; one-dimensional throat Mach number, 0.51; experimental separation.
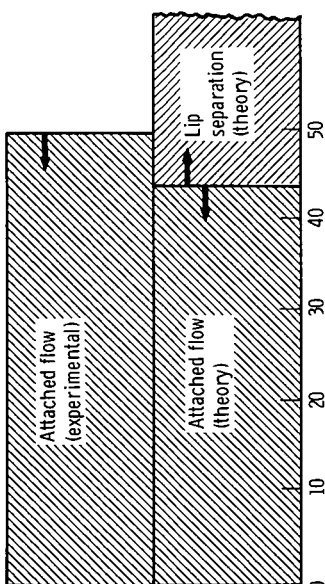
Figure 10. - Continued.

(d) Incidence angle, 50°; one-dimensional throat Mach number, 0.70; no experimental separation.
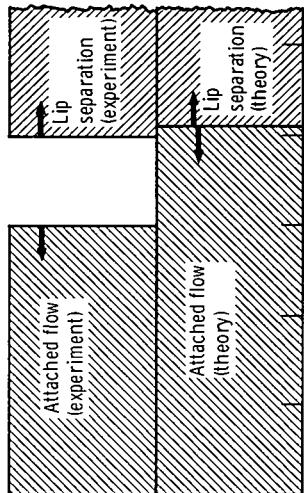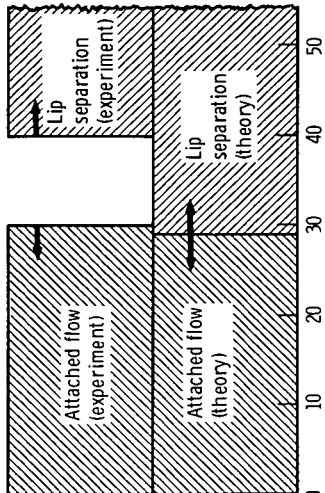
Figure 10. - Concluded.

(a) One-dimensional throat Mach number, 0.51.

(b) One-dimensional throat Mach number, 0.70.

Figure 12. - Summary of lip separation results for 1.35-contraction-ratio inlet.

(a) One-dimensional throat Mach number, 0.48.

(b) One-dimensional throat Mach number, 0.64.

Figure 11. - Summary of lip separation results for 1.26-contraction-ratio inlet.

"The aeronautical and space activities of the United States shall be conducted so as to contribute . . . to the expansion of human knowledge of phenomena in the atmosphere and space. The Administration shall provide for the widest practicable and appropriate dissemination of information concerning its activities and the results thereof."
—NATIONAL AERONAUTICS AND SPACE ACT OF 1958

NASA SCIENTIFIC AND TECHNICAL PUBLICATIONS

TECHNICAL REPORTS: Scientific and technical information considered important, complete, and a lasting contribution to existing knowledge.

TECHNICAL NOTES: Information less broad in scope but nevertheless of importance as a contribution to existing knowledge.

TECHNICAL MEMORANDUMS: Information receiving limited distribution because of preliminary data, security classification, or other reasons. Also includes conference proceedings with either limited or unlimited distribution.

CONTRACTOR REPORTS: Scientific and technical information generated under a NASA contract or grant and considered an important contribution to existing knowledge.

TECHNICAL TRANSLATIONS: Information published in a foreign language considered to merit NASA distribution in English.

SPECIAL PUBLICATIONS: Information derived from or of value to NASA activities. Publications include final reports of major projects, monographs, data compilations, handbooks, sourcebooks, and special bibliographies.

TECHNOLOGY UTILIZATION PUBLICATIONS: Information on technology used by NASA that may be of particular interest in commercial and other non-aerospace applications. Publications include Tech Briefs, Technology Utilization Reports and Technology Surveys.

Details on the availability of these publications may be obtained from:

SCIENTIFIC AND TECHNICAL INFORMATION OFFICE

NATIONAL AERONAUTICS AND SPACE ADMINISTRATION
Washington, D.C. 20546